Optics & Laser Technology 162 (2023) 109284

Contents lists available at ScienceDirect

Optics and Laser Technology

journal homepage: www.elsevier.com/locate/optlastec

Full length article

Polarization maintaining harmonically mode-locked fiber laser with suppressed supermode noise due to continuous wave injection

D.A. Korobko [a,*], V.A. Ribenek [a], P.A. Itrin [a], D.A. Stoliarov [a], A.A. Fotiadi [b,c,*]

[a] Ulyanovsk State University, 42 Leo Tolstoy Street, Ulyanovsk 432970, Russian Federation
[b] Optoelectronics and Measurement Techniques Unit, University of Oulu, Oulu, Finland
[c] Electromagnetism and Telecommunication Department, University of Mons, Mons B-7000, Belgium

ARTICLE INFO

Keywords:
Polarization maintaining fiber lasers
Harmonic mode-locking
Supermode noise suppression

ABSTRACT

We report on experimental studies of a SESAM mode-locked Er-doped fiber laser completely spliced from polarization-maintaining fiber components. With the fiber mode spot properly aligned to the SESAM, the laser operates harmonic mode-locking (HML) available in a whole range of pump powers up to ~355mW with the supermode suppression level (SSL) less than 25 dB. Importantly, the HML laser generates the pulses in a linear polarization state and enables the pulse repetition rate (PRR) up to ~1145 MHz. In our experiments we show that an optical injection of an external continuous wave (CW) into the laser cavity improves the stability of the laser operation in HML regime resulting in an increase of the SSL by 20–30 dB. Besides, the CW injection is able to expand the range of pump powers available with HML laser providing an increase of the maximal laser PRR up to ~2195 MHz. Importantly, the implemented optical injection does not affect high purity of the laser polarization state. The presented numerical simulations enable qualitative explanations of the effects observed experimentally.

1. Introduction

Ultra-fast laser sources delivering pulses with the pulse repetition rate (PRR) in sub-GHz and GHz ranges are of great interest for many applications in spectroscopy, microwave photonics, ranging sensing, telecommunications, etc. [1,2]. Passively mode-locked fiber lasers combining high beam quality, simplicity of adjustment, reliability, user-friendly fiber interface and relatively low cost are of great demand for these applications. Whereas the fundamental PRR in the mode-locked fiber lasers is limited by tens of MHz, the harmonic mode locking (HML) techniques providing an equalized distribution of multiple pulses in the fiber cavity offer the possibility to achieve the PRR of tens of GHz [3–6]. A major drawback of fiber-based HML lasers are their relatively high amplitude fluctuations and timing jitter that significantly exceeds the characteristics of the lasers operating the fundamental PRR [7]. Noise-induced perturbations of pulse train periodicity appear in the frequency domain as spurious supermodes with non-multiple PRR frequencies. The solutions enabling suppression of the supermode noise in HML fiber lasers are of great practical importance [8,9]. In particular, the optical injection from an external laser source could be used to control the fiber laser outputs. For example, the methods based on the heterochromic optical pulse injection have been reported for control of the mode-locking threshold [10] and pulse repetition rate [11,12] in the mode-locked fiber lasers.

In our recent experiments with a HML fiber laser based on nonlinear polarization evolution (NPE), we have demonstrated a new technique for the supermode noise suppression using aresonant optical injection from the external narrow-band continuous wave (CW) laser into the harmonically mode-locked laser cavity [13,14]. Specifically, to implement the effect the wavelength of the injected CW should be in a proximity to the long-wavelength spectral Kelly sideband. In this case, the interaction between the pulses and the injected CW results in their phase-matching with the formation of a united light structure (pulses + CW) enabling significant reduction of the supermode noise. In our experiments, the supermode noise suppression by more than 30 dB has been demonstrated with the NPE harmonically mode-locked fiber laser operating with the PRR ~1–2 GHz [14].

However, the fiber laser configurations mode-locked by NPE are not very practical since they too sensitive to the external environment and so require regular adjustment of the polarization controllers. Besides the spectrum of soliton fiber laser built on non-polarization maintaining (PM) components has additional sub-sidebands, and the polarization

* Corresponding authors.
E-mail addresses: korobkotam@rambler.ru (D.A. Korobko), Andrei.Fotiadi@oulu.fi (A.A. Fotiadi).

https://doi.org/10.1016/j.optlastec.2023.109284
Received 21 December 2022; Received in revised form 27 January 2023; Accepted 13 February 2023
Available online 21 February 2023

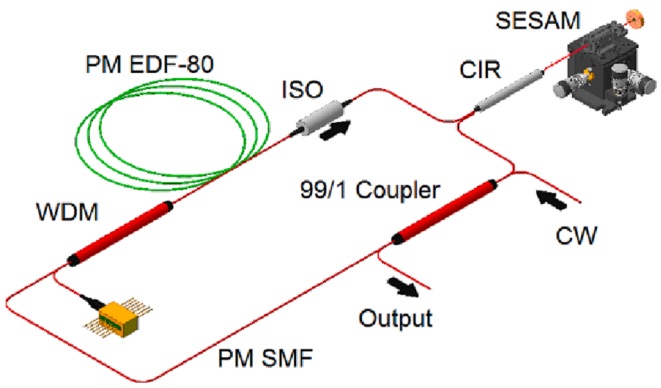

Fig. 1. Experimental setup.

state of the output pulses is constantly changing [15]. The all-PM laser configurations using special saturable absorber, for example, semiconductor mirror (SESAM) are free from these drawbacks and are able to deliver stable and pure linear polarized pulse trains. In this paper, we demonstrate that the method of supermode noise suppression we have implemented with NPE harmonically mode-locked fiber lasers is applicable for operation with the PM lasers harmonically mode-locked by SESAM as well. For this purpose, we present the results of our experiments with the SESAM-based PM laser configuration, including the effect of an optical injection from an external narrow-band tunable laser source on the laser performance characteristics. The numerical simulations are also provided to clarify the nature of the effect.

2. Experiment

The experimental laser configuration is shown in Fig. 1. The laser cavity is completely splices from PM fiber components. It comprises ~1.2 m long PM erbium doped fiber (Er80-4/125-HD-PM) with dispersion D = –22 ps/(nm km), a PM fiber isolator, 980/1550 PM single-mode WDM coupler and 1 % output coupler. The laser is mode-locked by SESAM (with the relaxation time of 4 ps) attached to the cavity through PM circulator and translation platform. The laser is pumped by a 980 nm laser diode with the maximal power of 900 mW. The total laser cavity length is ~9.2 m sets the fundamental laser PRR f_T = 22.4 MHz. The total cavity dispersion is anomalous, so the laser generates soliton pulses. The laser operation is monitored by an optical spectrum analyzer (Yokogawa 6370D) with resolution of 0.02 nm and RF spectrum analyzer (R&S FSP40) equipped with a 30 GHz photodetector.

When the pump power is increased up to ~105 mW, the laser starts is mode-locked at fundamental frequency at the wavelength $\lambda_0 \approx 1567$ nm. In the mode-locking regime the laser operation is not sensitive to the external disturbances of the cavity fibers.

Moreover, when the laser power is switched-off from this state and then switched-on the laser self-starts and restores the mode-locking regime. When the pump power is increased up to 112 mW, the laser begins to operate multi-pulses. A proper alinement of the fiber mode spot to the SESAM mirror in this case allows to equalize the pulse distribution inside the cavity, thus enabling HML laser operation. Again, once the HML regime is achieved, the laser is able to restore it after each restarting. Fig. 2 (a) shows the laser output power and PRR as functions on the pump power. One can see that both of them increase with the pump power almost linearly, but the PRR changes in stepwise manner since each step corresponds to the appearance of several (2–4) new pulses in the cavity. It is worth noting that the PRR steps measured with decreasing pump power differs from that shown in Fig. 2 due to the hysteresis effect that is typical for fiber lasers [16]. The range available for the HML laser operation is limited by the maximum PRR of ~1145 MHz achieved at the critical pump powerP_{cr} ~355 mW. Above this level the HML laser operation is destroyed and the laser operates chaotic pulse

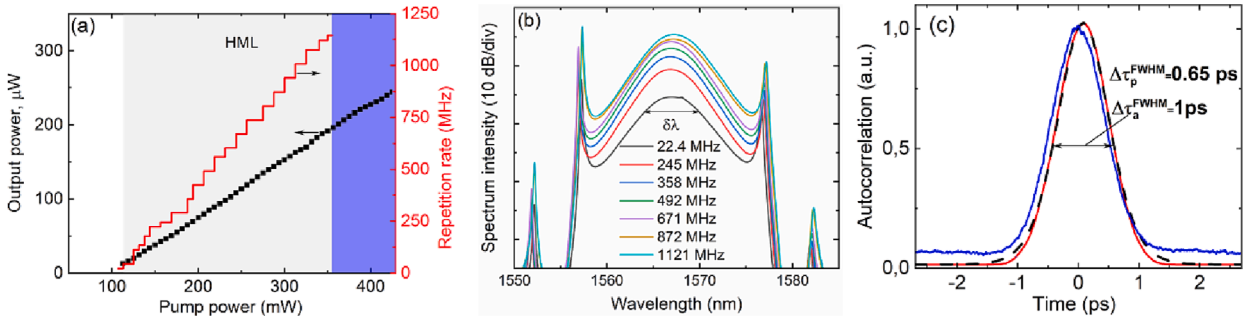

Fig. 2. (a) The output laser power (black squares) and PRR (red line) as functions of the pump power. The range available for HML generation is colored in gray, the range of the pulse bunch generation is blue colored. (b) Optical HML laser spectra recorded for different PRR. $\delta\lambda$ evaluates the 3 dB spectrum width. (c) Autocorrelation trace of the output laser pulse for PRR = 245 MHz without (red) and with CW injection (blue line). Dashed curve shows $sech^2$ fitting.

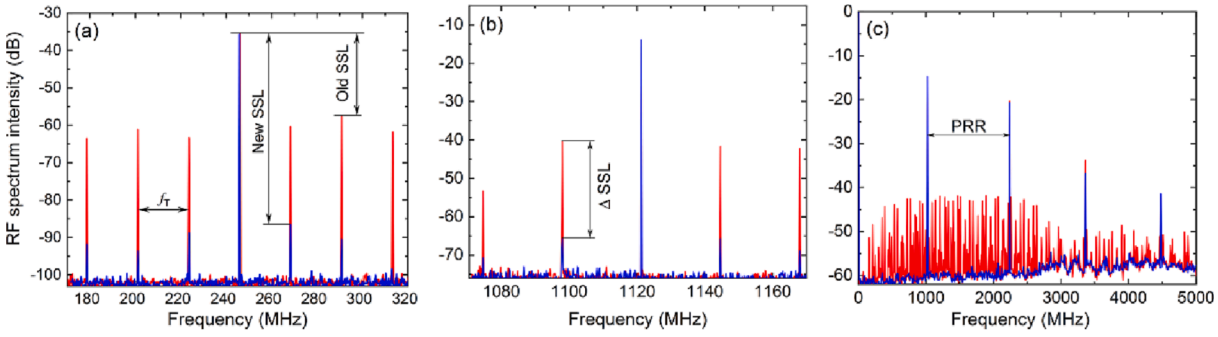

Fig. 3. The RF spectra of the HML laser without (red) and with the external CW injection (blue). The spectra are recorded with a 300 kHz resolution for PRR = 245 MHz (a) and PRR = 1121 MHz (b). The RF laser spectrum for PRR = 1121 MHz with a 10 MHz resolution (c).

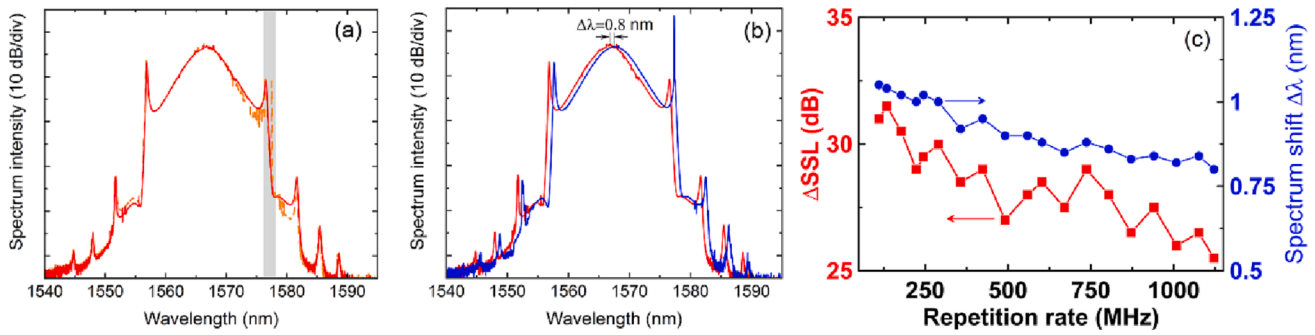

Fig. 4. (a) The laser optical spectra recorded for the PRR = 1121 MHz without CW injection (solid) and just after injection (dashed line). The grey line highlights the band where the CW injection causes a shift of the laser spectrum. (b) The optical spectrum shift caused by the CW injection at the PRR = 1121 MHz. Optical spectrum without (red) and with (blue) the CW injection at the wavelength enabling the maximal spectrum shift. (c) The changes of the supermode suppression level △SSL recorded with the RF spectrum analyzer with the resolution of 300 kHz (red squares) and maximal optical spectrum shifts $\Delta\lambda$ (blue circles) caused by the CW injection as functions of the laser PRR.

bunches.

The laser optical spectra measured for the different PRR are shown in Fig. 2 (b). One can see that the 3-dB spectrum width is ~6 nm for all measured spectra, i.e., it is almost independent on the PRR. It means that the single pulse energy is nearly the same within the HML area. The linear dependences of the output power and PRR on pump power are also in agreement with this statement. Note as well that all spectra exhibit pronounced Kelly sidebands that are features confirming the soliton nature of the pulses. Fig. 2 (c) (red line) presents the pulse autocorrelation traces recorded for PRR = 245 MHz One can see that the pulse shape is well approximated by sech^2 fitting with the pulse duration $\Delta\tau_p^{FWHM} \approx 0.65$ ps. The time-bandwidth product is of ~0.48 corresponding to the weakly chirped output pulse.

A typical radiofrequency (RF) spectrum of the HML laser comprises the main peaks and spurious supermode peaks surrounding them. The frequencies of the main peaks are multiples of the PRR, whereas the frequencies of supermode peaks are multiples of the fundamental frequency f_T. The integral intensity accumulated in the supermode peaks determines the laser pulse jitter, i.e., the fluctuations of pulse amplitudes and inter-pulse intervals in the HML pulse train [7].

Fig. 3 shows the RF laser spectra recorded for PRRs ~245 MHz and ~1121 MHz with different resolutions. The ratio between the main peak intensity and the maximal intensity of the surrounding supermodes evaluates the HML laser stability and is referred to as the supermode suppression level (SSL). One can see from the Fig. 3 (a) that the SSL for the PRR = 245 MHz is ~25 dB. It corresponds to moderate stability of the HML laser, the timing jitter measured directly by oscilloscope in this case is ~75 ps. Fig. 3 (b) gives similar characteristics for PRR = 1121 MHz: the SSL is ~23 dB, it corresponds to the experimentally measured timing jitter of ~56 ps.

A narrow-band optical radiation delivered by an external linearly polarized CW laser source Santec TSL is used for optical injection into the laser cavity. The CW laser is tunable in the range of 1480–1630 nm and set to operate with the linewidth of ~100 kHz and output power of ~10 mW. The CW light is injected into the HML laser cavity through the PM output coupler as it is shown in Fig. 1. The effect of the CW injection is monitored by the optical and RF spectrum analyzers scanning the CW laser in the wavelength range λ_{CW} 1550–1585 nm. We have found that the result of CW injection into the HML laser cavity depends on the position of the CW laser wavelength λ_{CW} relatively to the soliton pulse spectrum. In particular, close approaching the CW laser wavelength to the soliton spectrum maximum λ_0 perturbates the HML laser operation. The original laser spectrum and HML operation are restored immediately as the injection wavelength λ_{CW} is turned away fromλ_0. However, the most curious effects are observed when the CW wavelength is close to the Kelly sidebands of the HML laser optical spectrum as shown in Fig. 4.

When the CW wavelength λ_{CW} is critically approaching to the long-wavelength Kelly sideband (Fig. 4 (a)), the soliton spectrum is shifted as a whole towards the CW line such that the Kelly sideband and CW line are merged. Fig. 4 (b) compares the optical spectra recorded for the PRR = 1121 MHz observed without and with the CW injection. The corresponding RF spectra are shown in Fig. 3 (b). One can see that the optical injection induces the spectrum shift $\Delta\lambda = 0.8$ nm and simultaneously reduces the supermode noise by tens of dB. Fig. 3 (a) shows similar SSL increasing for the PRR ~245 MHz. One can see that the measured increases of the SSL due to resonant CW injection are Δ SSL = 29 dB for the PRR ~245 MHz and Δ SSL = 25.5 dB for the PRR = 1121 MHz. The recording of RF spectra with a 10 MHz resolution in a wide spectrum range gives Δ SSL = 18 dB for the PRR = 1121 MHz (Fig. 3 (c)). It is worth noting that these data are in agreement with the direct oscilloscope measurements of the timing jitter. The CW injection into the laser cavity causes reduction of the timing jitter down to the 8.5 ps for the PRR ~245 MHz and down to ~10.2 ps for the PRR ~1121 MHz. The autocorrelation trace for PRR = 245 MHz presented in Fig. 2 (c) (blue line) demonstrates that the CW injection affects neither the pulse shape nor the pulse duration. Also, one can see that CW injection leads to an increase of the radiation background compared to the case without CW injection. Similar experiments have been repeated for all PRRs available with the HML laser operation. Fig. 4 (c) shows the changes of the supermode noise suppression and maximum spectral shifts $\Delta\lambda$ recorded for different PRRs. One can see that the values of Δ SSL and $\Delta\lambda$ are in positive correlation and decrease together with the PRR increase.

One more effect of the resonant CW injection on the HML laser operation has been revealed. Without the CW injection the HML laser operation is limited by the maximum PRR = 1145 MHz achieved at the critical pump power level P_{cr} ~ 355 mW. Above this power$P > P_{cr}$, the laser generates chaotic pulse bunch (blue area in Fig. 2(a)). We have found that at $P > P_{cr}$ the resonant CW injection close to the long-wavelength Kelly sideband could stabilize the laser operation triggering its transition to the HML generation regime. The PRR in this case is determined by the pump power level that could be gradually adjusted to control the laser PRR available up to ~2 195 MHz with the pump power of ~630 mW. It is worth noting that an additional alinement of the fiber mode spot to the SESAM could be sometimes required to keep the HML generation.

We have also observed that the CW injection close to the short-wavelength Kelly sideband does not improve the HML laser performance. The effect of such injection is available in a whole HML laser operation range and is similar to that reported with the laser harmonically mode-locked by NPE [13]. As in the case of long-wavelength Kelly sideband, with the CW laser wavelength approaching to the short-wavelength Kelly sideband the optical spectrum shifts towards the CW such that the CW line and Kelly sideband merge. However, in contrast to

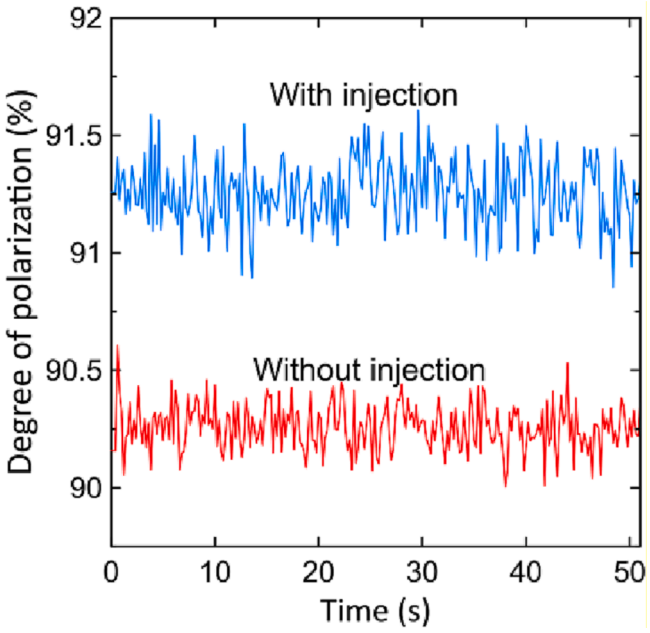

Fig. 5. Temporal evolution of the degree of polarization recorded with the HML laser delivered the pulses with the PRR = 1121 MHz without (red) and with (blue) the resonant CW injection into the long-wavelength Kelly sideband.

that case this process destroys the HML laser operation transforming it into generation of the chaotic pulse bunch.

Finally, we have used a polarimeter Keysight N7781B to evaluate the polarization state of the HML laser. Fig. 5 shows the degree of polarization measured for the laser operating in the HML regime with the PRR = 1121 MHz. One can see that without CW injection the degree of polarization is at the level of 90.3 % with 0.3 % variation over 50 s measurement time. When the CW is injected closely to the long-wavelength Kelly sideband the degree of polarization increases to the level of ~91.25 % but the variation also grows to the value of ~0.4 %. So, we can conclude that the laser demonstrates satisfactory polarization stability and CW injection improves the linear polarization state of the laser.

3. Numerical simulations

In the previous section we have demonstrated experimentally that the CW injection at the wavelength close to the long-wavelength Kelly sideband improves the quality of the HML in the PM fiber laser operation leading to the significant reduction of the supermode noise. In this section we present numerical simulations that help to clarify the nature of the effect. It is well known that the equalized pulse distribution in HML ring fiber laser cavity is a result of the mutual repulsion [17,18]. Weak pulse repulsion leads to the pulse train disordering as it is not able to restrain the pulse disturbances induced by the laser noise or competitive attraction forces. A typical example of such competing interactions is the repulsion forces induced by gain depletion and recovery mechanism [17] and attraction forces induced by the pulse interaction through the dispersion waves [19]. We believe that the stabilization of the HML observed in the experiment with PM fiber laser occurs due to the fact that the resonant CW injection is able to reinforce the pulse repulsion in the laser cavity. To demonstrate this idea, we have performed numerical simulations to compare the process of the HML pulse equalization in a PM fiber cavity with and without the resonant CW injection. The key challenge of these simulations is to determine the factors affecting the strength of the interpulse interaction in the fiber cavity without exact replication of the experimental conditions avoiding too complicated and time-consuming calculations. Therefore, we

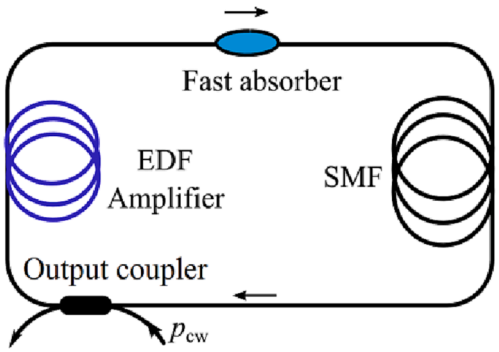

Fig. 6. The laser scheme used for numerical simulations.

consider only two pulses propagating in the ring cavity and apply a few simplifications. The principal laser configuration used for the simulation is shown in Fig. 6.

The light propagation through the segments of PM fibers of lengths l_{EDF} (EDF) and l_{SMF} (SMF) is described by equation of the NLS type:

$$\frac{\partial A}{\partial z} - i\frac{\beta_2}{2}\frac{\partial^2 A}{\partial t^2} - i\gamma|A|^2 A = \frac{gA}{2} + \frac{\beta_{2f}}{2}\frac{\partial^2 A}{\partial t^2}, \quad (1)$$

where $A(z,t)$ is the light amplitude. The fiber group velocity dispersion β_2 and the Kerr nonlinearity γ are assumed to be equal in the EDF and SMF for simplicity (in the SMF the gain and filtration are set to $g = \beta_{2f} = 0$). All the linear losses are accounted by the output coupler described by the coefficient$\rho < 1$. Fast saturable absorber is described by the transfer function using the instantaneous relaxation model.

$$F_{SA} = 1 - \alpha_{NS} - \frac{\alpha_0}{1 + |A|^2/P_s}$$

where α_{NS}– is the non-saturated loss, α_0– is the saturable absorber modulation depth and P_s – is the saturation power.

In the HML fiber lasers operating with PRR ranging in $10^2 - 10^4$ MHz the pulse repulsion is governed mainly by the gain depletion and recovery [18]. In order to simplify the simulation it is convenient to represent the fiber gain isolating its time-dependent part$g(z,t) = g_s(z) + g_t(t,z), \quad g_s \gg g_t$. In this case, the steady-state gain g_s is the gain factor averaged over the simulation window

$$g_s(z) = g_{s0}\left(1 + \frac{1}{E_g}\int_0^{\tau_{win}} |A(z,t)|^2 dt\right)^{-1} \quad (2)$$

Here g_{s0} – is the small signal gain, E_g – is the saturation energy determined by the pump power. In spectral domain the g_s is assumed to has a parabolic profile centered at the wavelength $\lambda = 1560$ nm and with the filter band $\beta_{2f} = g_s/\Omega_g^2$ determined by the gain spectrum widthΩ_g.

The repulsion between the pulses in the HML laser cavity is governed by the time-dependent gain $g_t(t,z)$ obeying the saturation and relaxation described as

$$\frac{dg_t}{dt} = \frac{g_{t0} - g_t}{\tau_g} - \frac{g_t|A(z,t)|^2}{E_g} \quad (3)$$

where the parameter $g_{t0} << g_{s0}$ denotes the non-saturated limit of the time-dependent gain$g_t(t,z)$, τ_g is the gain relaxation time. Considering the gain decrease caused by passing a single pulse Δg_t one can check that the time-dependent gain provides a pulse group-velocity drift proportional toΔg_t. For the pulses non-uniformly distributed in the cavity, the differences in the pulse velocity drifts lead to the mutual repulsion resulting in equalization of the interpulse intervals characterizing the HML pulse arrangement [17].

The amplitude A_{CW} of the CW wave injected into the system through the output coupler reads as

Table 1

Parameter	Value	Parameter	Value	Parameter	Value
$\gamma(W^{-1}\,m^{-1})$	0.0033	$g_{s0}(m^{-1})$	0.15	α_0	0.025
$\beta_2(ps^2m^{-1})$	−0.018	$g_{t0}(m^{-1})$	0.025	α_{NS}	0.125
$\Omega_g/2\pi$(THz)	2.25	E_g(pJ)	115	P_s(W)	5
l_{SMF}(m)	10	τ_g(ns)	75	ρ	0.9
l_{EDF}(m)	2.5	τ_{win}(ps)	246	p_{CW}(mW)	0.75

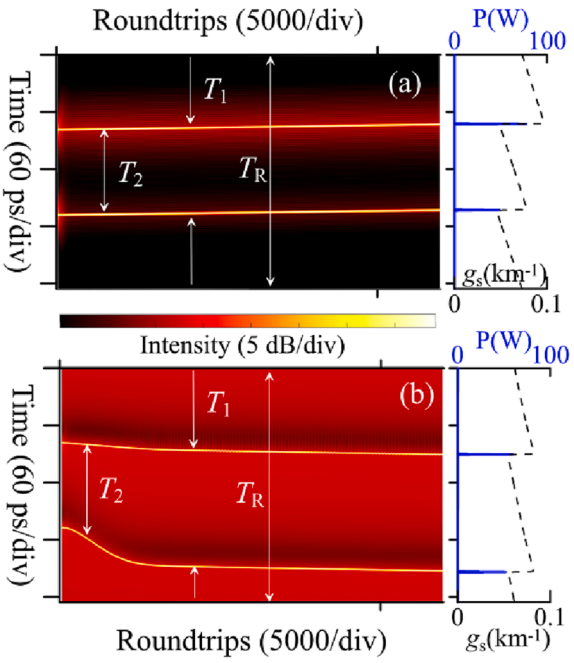

Fig. 7. The result of numerical simulations describing evolution of two pulses propagating in the PM fiber laser cavity. The pulses interact through the gain depletion and recovery mechanism without (a) and with (b) the CW injection. On the right, the final pulse arrangement and the time-dependent gain $g_s(t)$ are shown.

$$A(t,k) = \rho A(t,k-1) + \sqrt{1-\rho^2}A_{CW}(t,k) \tag{4a}$$

where ρ is the coupling coefficient, k is the cavity roundtrip number ($k = 1..\infty$). The resonant cavity conditions are satisfied by using the following relation.

$$A_{CW}(t,k) = \sqrt{p_{CW}}\exp\left(i\left(\omega_{CW}t + \beta_2\omega_{CW}^2(l_{SMF}+l_a)(k-1)/2\right)\right) \tag{4b}$$

where p_{CW} is the CW injection power and ω_{CW} is the CW frequency offset from the peak gain frequency. The values of the system parameters used for calculations are shown in Table 1.

In our simulations the ring fiber cavity containing two soliton pulses that interact through the gain depletion and recovery is considered as a time window with periodic boundary conditions. The size of the simulation window is equal to the fundamental cavity period $\tau_{win} = T_R = 1/f_T$. Although in real fiber laser systems $T_R \sim 100$ ns and Er-doped fibers are characterized by the relaxation time $\tau_g \sim 0.1$ ms, i.e., $T_R << \tau_g$, we have accelerated the calculations using the scaled time parameters ($T_R \sim 10^{-10}$s, $\tau_g \sim 10^{-7}$s). So, all real processes in fiber lasers are $\sim 10^2$–10^3 times slower than that obtained in simulations.

Fig. 7 compares the system evolution governed by the time-dependent gain alone (a) and in combination with the resonant CW injection (b). In both cases there are two soliton pulses travelling in the cavity. Their mutual position is described by the intervals between them T_1 and $T_2 = T_R - T_1$. We suppose that at the initial moment of time ($t = 0$) two soliton pulses are not nonequally spaced in the cavity setting $T_{10} = 156$ ps and $T_{20} = T_R - T_{10} = 90$ ps. The time-dependent gain alone

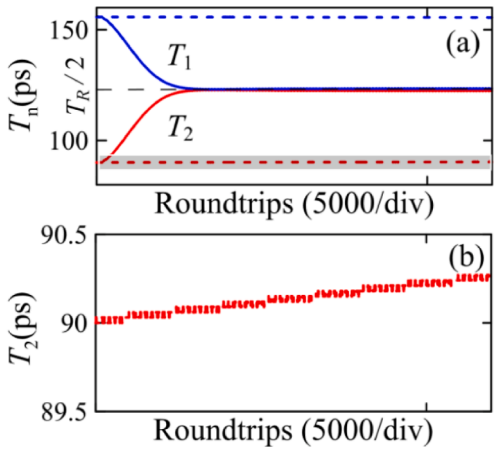

Fig. 8. (a) The result of numerical simulations describing evolution of the time intervals between two pulses propagating in the PM fiber laser cavity. The pulses interact through the gain depletion and recovery without (dashed line) and with (solid line) the CW injection. (b) Zoom-in image of the Fig. 8 (a) marked area.

operates to arrange the pulses equidistantly, when $T_2 = T_1$, but one can see that in this case, the time intervals between the pulses change pretty slowly. Fig. 8(a, b) highlight details of this evolution: the difference $|T_2 - T_1|$ changes for 5000 cavity roundtrips by less than 1 ps. In this case, the pulse repulsion is relatively weak to significantly suppress the laser noise disturbing the pulse periodicity and determining timing jitter in the HML laser.

For the simulations performed with the CW injection, the frequency $\omega_{CW} \approx -6.7{\cdot}10^{12}s^{-1}$ has been set close to the position of the long-wavelength Kelly sideband of the soliton spectrum ($\omega_K \approx -6.65{\cdot}10^{12}s^{-1}$). Fig. 7(b) demonstrates a much more intensive evolution of two pulses arrangement resulting in fast equalization of interpulse intervals in the cavity. The difference $|T_2 - T_1|$ shown in Fig. 8(a) (solid lines) changes smoothly but rapidly approaches zero for less than 2000 cavity roundtrips. This system evolution testifies to the strong repulsion between the pulses in the HML laser cavity enabling much more significant suppression of the laser noise than in the first case.

To explore the details of the effect on the resonant CW injection operating in combination with the time-dependent gain on the repulsion or attraction between pulses in the ring laser cavity, we have analyzed the interaction between the pulses and background originated from injected radiation. Without the time-dependent gain and CW injection both pulses in the cavity experience equal gains on their mutual position. As it has been mentioned above the implementation of the gain depletion and recovery into the system makes the local gain applying to a pulse dependent on the position of the previous pulse thus resulting in equalization of the interpulse intervals [17].

The CW injection into the laser cavity may accelerate or annihilate this pulse equalization process [13] providing additional modulation to the time-dependent gain that, in turn, controls the group velocity of each pulse. The reason for this extra modulation is the specific shape of the pulse pedestal that the resonant CW injection forms due to its interference with the original dispersive wave produced by the pulse. It is known that the soliton pedestal is the dispersive wave generated due to periodic amplification and decay of the pulse propagating through the lumped cavity elements. The dispersive waves are observed as the Kelly sidebands in the spectral domain [20]. In the fiber cavity with an anomalous dispersion the long- and short- wavelength Kelly sidebands are associated with the dispersive waves forming the left and right wings of the pulse pedestal, respectively. So, when the injection wavelength λ_{CW} is close to one of the Kelly sidebands a stable asymmetric interference pattern is generated. With the CW component close to the long-

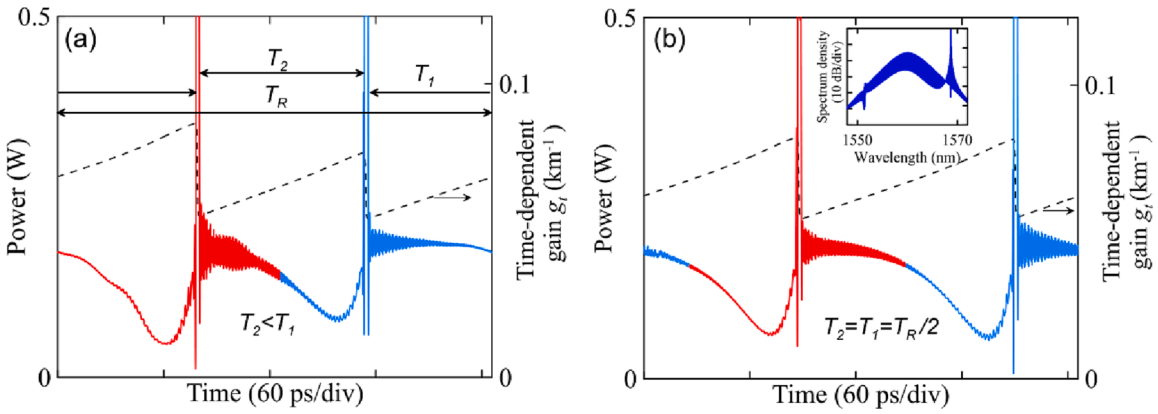

Fig. 9. Pedestals of the pulse pair interacting through the time dependent gain g_t alone and with the CW injection into the long-wavelength Kelly sideband. (a) Early stage of the interaction. (b) The stage close to the equilibrium point. The optical laser spectrum is shown in the inset.

wavelength sideband (Fig. 9) the destructive interference reduces the pedestal intensity at the left soliton wing [21], resulting in the less depleted time-dependent gain spurring the pulse and an additional increase of the pulse group velocity. The higher reduction of the pedestal level preceding the pulse, the more considerable income the pulse group velocity gets. The longer spacing between pulses enables a more significant decrease of the pedestal level. Therefore, the pulse following the longer interpulse spacing gets the more considerable income to the pulse group velocity, i.e. the cooperative action of the CW injection and time-dependent gain provides the velocity drifts enabling the reinforcement of the repulsion and resulting in the final pattern with repeatability of the pedestal profile. When the resonant CW is injected close to the short-wavelength Kelly sideband its destructive interference with the dispersive wave reduces the pedestal intensity at the soliton right pedestal wing [21], resulting in an increase of the group velocity for the next pulse. This mechanism enables attraction between pulses thus operating against the repulsion provided by the gain depletion and recovery mechanism. Their cooperative action destroys the HML operation leading to the formation of pulse bunch observed in the experiment.

4. Conclusion

The technique of supermode noise suppression we have proposed recently and implemented with fiber lasers harmonically mode-locked by NPE [13,14] is extended now for operation with the SESAM-based fiber laser configuration completely spliced from polarization-maintaining fiber components. With the mode spot area properly aligned with the SESAM the laser exhibits the HML operation available in a whole range of the pump powers up toP_{cr} ~355mW. Importantly, the laser generates the pulses in a linear polarization state and enables the pulse repetition rate (PRR) up to ~1145 MHz. The HML laser operation is characterized by a moderate SSL value ~25 dB that slightly decreases with the PRR increase. When the pump power exceeds the critical level$P > P_{cr}$, the laser switches to generate a bunch of pulses.

We have experimentally demonstrated that the CW injection close to the long-wavelength Kelly sideband improves the stability of the laser operation in HML regime resulting in an increase of the SSL by 20–30 dB. Moreover, the CW injection expands the range of the pump powers available for HML laser operation and increases the maximum laser PRR up to ~2195 MHz. Importantly, the implemented procedure does not affect high purity of the laser linear polarization state. It has been as well demonstrated that the similar CW injection into the short-wavelength Kelly sideband leads to destruction of the HML laser operation.

The performed numerical simulations support ideas for qualitative explanations of the observed effects induced by the resonant CW injection. We have demonstrated that the CW injection triggers additional mechanisms affecting the strength of interaction forces between the pulses inside the fiber cavity. The resonant CW injection to the long-wavelength Kelly sideband leads to the appearance of additional repulsive force increasing the stability of the HML laser operation. In contrast, the resonant CW injection to the short-wavelength Kelly sideband causes pulse attraction forces that annihilate the pulse repulsion provided by the gain depletion and recovery mechanism. It destroys the HML laser operation leading to the formation of pulse bunch. We believe that our new findings will facilitate the design of self-stabilized internally PM fiber lasers operating with an extended diversity of the laser performance characteristics [22–24] and demanded for many practical laser applications.

Funding:

This work is supported by the Ministry of Science and Higher Education of the Russian Federation (075-15-2021-581) and Russian Science Foundation (grant # 22-72-10072). A.A.F. is supported by the European Union's Horizon 2020 research and innovation program (H2020-MSCA-IF-2020, #101028712).

CRediT authorship contribution statement

D.A. Korobko: Investigation, Formal analysis, Validation, Methodology, Software, Writing – original draft. **V.A. Ribenek:** Investigation, Validation, Methodology. **P.A. Itrin:** Investigation, Validation, Data curation. **D.A. Stoliarov:** Investigation, Validation, Methodology. **A.A. Fotiadi:** Supervision, Writing – original draft.

Declaration of Competing Interest

The authors declare that they have no known competing financial interests or personal relationships that could have appeared to influence the work reported in this paper.

Data availability

Data will be made available on request.

References

[1] V. Torres-Company, A.M. Weiner, Optical frequency comb technology for ultra-broadband radio-frequency photonics, Laser Photonics Rev. 8 (3) (2014) 368–393.
[2] T. Fortier, E. Baumann, 20 years of developments in optical frequency comb technology and applications, Commun. Phys. 2 (1) (2019) 1–16.
[3] A.B. Grudinin, S. Gray, Passive harmonic mode locking in soliton fiber lasers, JOSA B 14 (1) (1997) 144–154.
[4] J. Bogusławski, G. Soboń, R. Zybała, J. Sotor, Towards an optimum saturable absorber for the multi-gigahertz harmonic mode locking of fiber lasers, Photonics Res. 7 (9) (2019) 1094–1100.
[5] C. Lecaplain, P. Grelu, Multi-gigahertz repetition-rate-selectable passive harmonic mode locking of a fiber laser, Opt. Express 21 (9) (2013) 10897–10902.

[6] D.A. Korobko, D.A. Stoliarov, P.A. Itrin, M.A. Odnoblyudov, A.B. Petrov, R. V. Gumenyuk, Harmonic mode-locking fiber ring laser with a pulse repetition rate up to 12 GHz, Opt. Laser Technol. 133 (2021), 106526.
[7] F. Rana, H.L. Lee, R.J. Ram, M.E. Grein, L.A. Jiang, E.P. Ippen, H.A. Haus, Characterization of the noise and correlations in harmonically mode-locked lasers, JOSA B 19 (11) (2002) 2609–2621.
[8] O. Pottiez, O. Deparis, R. Kiyan, M. Haelterman, P. Emplit, P. Mégret, M. Blondel, Supermode noise of harmonically mode-locked erbium fiber lasers with composite cavity, IEEE J. Quantum Electron. 38 (3) (2002) 252–259.
[9] G.R. Lin, M.C. Wu, Y.C. Chang, Suppression of phase and supermode noise in a harmonic mode-locked erbium-doped fiber laser with a semiconductor-optical-amplifier-based high-pass filter, Opt. Lett. 30 (14) (2005) 1834–1836.
[10] K. Yang, J. Li, J. Wu, A. Hu, Q. Hao, J. Peng, H. Zeng, Mode-locking threshold decrease in a fiber laser by heterochromic optical pulse injection, Opt. Lett. 47 (16) (2022) 4095–4098.
[11] T. Yu, J. Fang, Q. Hao, K. Yang, M. Yan, K. Huang, H. Zeng, High-precision passive stabilization of repetition rate for a mode-locked fiber laser based on optical pulse injection, Opt. Express 29 (13) (2021) 20930–20940.
[12] K. Yang, Y. Shen, J. Ao, S. Zheng, Q. Hao, K. Huang, H. Zeng, Passively synchronized mode-locked fiber lasers for coherent anti-Stokes Raman imaging, Opt. Express 28 (9) (2020) 13721–13730.
[13] D.A. Korobko, V.A. Ribenek, D.A. Stoliarov, P. Mégret, A.A. Fotiadi, Resonantly induced mitigation of supermode noise in a harmonically mode-locked fiber laser: revealing the underlying mechanisms, Opt. Express 30 (10) (2022) 17243–17258.
[14] V.A. Ribenek, D.A. Stoliarov, D.A. Korobko, A.A. Fotiadi, Mitigation of the supermode noise in a harmonically mode-locked ring fiber laser using optical injection, Opt. Lett. 46 (22) (2021) 5747–5750.
[15] G. Sobon, J. Sotor, K.M. Abramski, All-polarization maintaining femtosecond Er-doped fiber laser mode-locked by graphene saturable absorber, Laser Phys. Lett. 9 (8) (2012) 581.
[16] D.Y. Tang, L.M. Zhao, B. Zhao, A.Q. Liu, Mechanism of multisoliton formation and soliton energy quantization in passively mode-locked fiber lasers, Phys. Rev. A 72 (4) (2005), 043816.
[17] J.N. Kutz, B.C. Collings, K. Bergman, W.H. Knox, Stabilized pulse spacing in soliton lasers due to gain depletion and recovery, IEEE J. Quantum Electron. 34 (9) (1998) 1749–1757.
[18] X. Liu, M. Pang, Revealing the buildup dynamics of harmonic mode-locking states in ultrafast lasers, Laser Photonics Rev. 13 (9) (2019) 1800333.
[19] Y. Chen, M. Wu, P. Tang, S. Chen, J. Du, G. Jiang, S. Wen, The formation of various multi-soliton patterns and noise-like pulse in a fiber laser passively mode-locked by a topological insulator based saturable absorber, Laser Phys. Lett. 11 (5) (2014), 055101.
[20] M.L. Dennis, I.N. Duling, Experimental study of sideband generation in femtosecond fiber lasers, IEEE J. Quantum Electron. 30 (6) (1994) 1469–1477.
[21] A. Komarov, K. Komarov, A. Niang, F. Sanchez, Nature of soliton interaction in fiber lasers with continuous external optical injection, Phys. Rev. A 89 (1) (2014), 013833.
[22] D.C. Kirsch, A. Bednyakova, P. Varak, P. Honzatko, B. Cadier, T. Robin, A. Fotiadi, P. Peterka, M. Chernysheva, Gain-controlled broadband tuneability in self-mode-locked Thulium-doped fibre laser, Commun. Phys. 5 (2022) 219.
[23] H.J. Kbashi, S.V. Sergeyev, M. Al-Araimi, A. Rozhin, D. Korobko, A. Fotiadi, High-frequency vector harmonic mode locking driven by acoustic resonances, Opt. Lett. 44 (2019) 5112–5115.
[24] S. Boivinet, J.-B. Lecourt, Y. Hernandez, A.A. Fotiadi, M. Wuilpart, P. Megret, All-fiber 1-μm PM mode-lock laser delivering picosecond pulses at sub-MHz repetition rate, IEEE Photon. Technol. Lett. 26 (2014) 2256–2259.